E-COSM – Rencontres Scientifiques de l'IFP – 2-4 Octobre 2006, Proceedings, pp. 111-119

Airpath strategy for experimental control of a Diesel HCCI Engine

J. Chauvin[1,2*], G. Corde[1], N. Petit[2] and P. Rouchon[2]

1 Institut français du pétrole, 1 et 4, avenue de Bois-Préau, 92852 Rueil-Malmaison Cedex - France
2 Centre Automatique et Systèmes, École des Mines de Paris, 60 blvd Saint Michel, 75006 Paris
e-mail: jonathan.chauvin@ifp.fr - gilles.corde@ifp.fr - petit@cas.ensmp.fr - rouchon@cas.ensmp.fr
* Corresponding author

Abstract *— A motion planning based control strategy is proposed for the airpath control of turbocharged Diesel engines using exhaust gas recirculation (EGR). The considered model uses simple balance equations. The fully actuated dynamics are easily inverted, yielding straightforward open-loop control laws. This approach is complemented by experimentally derived look-up tables to cast the drivers requests into transients between operating points. Estimation of required variables is addressed and experimental tests are reported on a 4-cylinder engine in Homogeneous Charge Compression Ignition (HCCI) mode. Conclusions stress the possibility of taking into account the non-minimum phase effects of this system by a simple, yet efficient in practice, control law. Observed transients are accurate and fast.*
Keywords: Engine Control, Airpath, Motion planning, HCCI

1 INTRODUCTION

Increasingly stringent pollution standards norms have spurred a broad interest in the reduction of global engine emissions. Lately, two strategies have emerged: after-treatment and direct combustion emissions reduction. For Diesel engines, equipments required by after-treatment and implementation issues usually carry high cost premiums. An alternative is to use a cleaner combustion mode. Therefore, the Highly Premixed Combustion mode (HPC) – including Homogeneous Charge Compression Ignition (HCCI) – has become of major interest in recent years. It requires the use of high Exhaust Gas Recirculation (EGR) rates. The key idea is that the inert burnt gas (coming from the recirculation of cooled exhaust gas) in the cylinder lower the temperature and dilute the air charge which reduce the emissions of nitrogen oxides. In practice, numerous experimentations brought the proof of significant emission reduction (see [1,2] for example). Yet, actual vehicle implementation implies frequent transients which reveal to be much more complex than steady state experimentation.

As studied in [3,4], the airpath system of a turbocharged Diesel engine features coupled dynamics. The EGR acts as a discharge valve for the turbocharger. Most studies consider the following control setup: both intake pressure and intake air flow are closely controlled using EGR valve and Variable Geometry Turbocharger (VGT) using gain scheduling PI controllers as in [5,6,7]. The PI gains are tuned with respect of engine speed and fueling rate. PI gains are generated by the inverted plant gain at each operating point. Linear Parameter-Varying (LPV) formulation is used in [8,9]. A LPV Diesel airpath model is derived from a simple nonlinear system and use H_∞ loopshaping control to regulate the intake pressure and the intake air flow. Controlling both intake and exhaust pressure has been exposed in [10]. In [11,12], constructive Lyapunov technique is used to control the air-fuel ratio and EGR fraction to their respective set points determined by the operating

conditions during quasi-steady state operation. For that purpose, intake pressure, intake mass air flow, and exhaust pressure measurements are used along with several change of coordinates.

All these studies prove the relevance of multivariable control strategies. In this paper, we use a motion planning strategy and explicit a feedforward term. Originally, our objective is to satisfy the drivers's torque demand. Successively, we cast it into in-cylinder masses setpoints, and into BGR and intake manifold pressure control objective. An explicit unconstrained transient is computed. Hopefully, thanks to tuning parameters, it is consistent with physically important constraints on the inputs. If not, it is saturated, and, as is proven, eventually provides convergence anyway.

The contribution of this paper is as follows. We present the overall control scheme for the airpath control of a turbocharged Diesel engine. Extensive experimental results are reported. At the light of this study, we can finally conclude, with supportive results, that motion planning is indeed an appropriate solution for controlling the airpath dynamics.

The chapter is organized as follows. In Section 2, we detail the control problem. In Section 5, we decouple the airpath fully actuated dynamics by a simple motion planning strategy. Physical input constraints are explicited in the motion planning strategy. Closed loop controller design is presented in Section 6. Experimental results are reported on a 4 cylinder HCCI engine in Section 7. Conclusions and future directions are given in Section 8.

2 CONTROL PROBLEM

This macroscopic approach is sufficient for a first order NO_x reduction. Our approach to combustion control is to manage the air and burned gas masses in the cylinder ($M_{air,cyl}$ and $M_{bg,cyl}$). In other words, we focus on the airpath system. Flows of fresh air and the Exhaust Gas Recirculation (EGR) mix into the intake manifold and are aspirated into the cylinders. In practical applications, the considered masses can not be measured. Yet, equivalent variables can be considered. Controlling those two masses is equivalent to controlling the intake pressure P_{int} (being an image of $M_{air,cyl} + M_{bg,cyl}$) and the burned gas rate F_{int} (representing to ratio $\frac{M_{bg,cyl}}{M_{air,cyl}+M_{bg,cyl}}$). Setpoints are often chosen to maximize EGR in order to lower the NO_x emissions at low load. At high load, the EGR decreases the efficiency and imposes the use of low EGR. Typically, the setpoint at 1500 rpm and high load is ($P_{int,sp} = 2$bar, $F_{int,sp} = .05$) using low EGR, while at 1500 rpm and low load setpoints under consideration are close to ($P_{int,sp} = 1.013$bar, $F_{int,sp} = .45$) using high EGR.

In this context, the control problem we need to address is a large transient problem for a two outputs, two inputs system. The control inputs are the VGT actuator position $S_{vgt}(v_1)$ (ranging from 0 to 1) and the EGR valve normalized effective area $S_{egr}(v_2)$ (ranging from 0 to 1). Both are bounded. Other external inputs include the fueling rate M_{fuel} and the engine speed N_e. The underlying dynamics is also of dimension 2. The states are the outputs: P_{int} and F_{int}.

3 INTAKE MANIFOLD MODELLING

Flows from the fresh air (measured by the Manifold Air Flow) and the Exhaust Gas Recirculation (EGR) come into the intake manifold and are aspirated into the cylinders. For modelling, we use mass balances, ideal gas law, and consider a low time resolution (180^o TDC time scale). In particular, high frequency aspiration phenomena are not taken into account. A nomenclature is presented in Table 1.

Symb.	Quantity	Unit
P_{int}	Pressure in the i.m.	Pa
T_{int}	Temperature in the i.m.	K
M_{int}	Total mass in the i.m.	kg
$M_{int,air}$	Air mass in the i.m.	kg
V_{int}	i.m. volume	L
N_e	Engine Speed	rpm
D_{air}	Manifold air flow	kg.s^{-1}
D_{egr}	EGR flow	kg.s^{-1}
D_{asp}	Flow aspirated into the cylinders	kg.s^{-1}
V_{cyl}	Cylinders volume	L
γ_{int}	Specific heats ratio (i.m.)	-
F_{int}	Burned gas fraction in the i.m.	-
F_{exh}	Burned gas fraction in the e.m.	-
R	Ideal gas constant	J.(kgK)$^{-1}$
η_{vol}	Volumetric efficiency	-
u	EGR valve	-
	normalized effective area	

TABLE 1

Nomenclature. i.m. and e.m refer to the intake and exhaust manifold respectively.

Ideal gas law in the intake manifold leads to

$$P_{int}V_{int} = M_{int}RT_{int}$$

Assuming that the variation of temperature is slow (i.e. $\dot{T}_{int} = 0$), the mass balance writes

$$\dot{P}_{int} = \frac{R}{V_{int}}(D_{air} + D_{egr} - D_{asp}) \quad (1)$$

Classically (see [13] for exemple), we define the aspirated flow as

$$D_{asp} = \eta_{vol}(P_{int}, N_e)\frac{P_{int}}{RT_{int}}V_{cyl}\frac{N_e}{120} \quad (2)$$

where $V_{\rm cyl}$ is the cylinder volume. η_{vol} is the volumetric efficiency which is experimentally derived and, eventually,

defined though a look-up table $\eta_{vol,map}(P_{int}, N_e)$. Values vary with engine operating conditions (mainly intake pressure and engine speed).

The burned gas ratio F_{int} is the fraction of burned gas in the intake manifold. It writes

$$F_{int} \triangleq 1 - \frac{M_{int,air}}{M_{int}}$$

The composition of the EGR (F_{egr}) is the composition in the exhaust manifold (F_{exh}) delayed by the transport through the EGR pipe. We consider that this delay is negligible, i.e. $F_{egr} = F_{exh}$. Mixing dynamics is modelled as

$$\dot{F}_{int} = \frac{RT_{int}}{P_{int}V_{int}}(D_{egr}(F_{exh} - F_{int}) - D_{air}F_{int}) \quad (3)$$

The EGR flow can be expressed

$$D_{egr} = S_{egr}\frac{P_{exh}}{\sqrt{RT_{exh}}}\sqrt{\frac{2\gamma}{\gamma-1}(p_r^{\frac{2}{\gamma}} - p_r^{\frac{\gamma-1}{\gamma}})}$$

where $p_r = \max\{\frac{P_{int}}{P_{exh}}, (\frac{2}{\gamma+1})^{\frac{\gamma}{\gamma+1}}\}$. These two variables describe both subsonic and choked EGR flow. In this model, numerous variables are not measured. The exhaust pressure and temperature for example are not easily available on a commercial engine. The effect of the EGR cooler is accounted for by considering

$$D_{egr} \triangleq \Theta_{egr}S_{egr}$$

where Θ_{egr} is a variable depending on the exhaust temperature, the pressure ratio between intake and exhaust manifold, and the behavior of the cooling system. This variable need to be estimated to evaluate the EGR flow and the composition in the intake manifold, this is the purpose of the following Section.

4 AIR PATH OBSERVER

In this section we design an observer to estimate both the EGR flow and the BGR.

4.1 Reference Model

Let

$$x = \begin{bmatrix} P_{int} & F_{int} & \Theta_{egr} \end{bmatrix}^T \in \mathbb{R}^3$$

be the state and $y = P_{int}$ the measurement. We note $\alpha_{int} \triangleq \frac{RT_{int}}{V_{int}}$ and $\beta_{int} \triangleq \frac{1}{RT_{int}}V_{cyl}\frac{N_e}{120}$. Using (1) and (3), the reference dynamics reads

$$\begin{cases} \dot{x}_1 = \alpha_{int}\left(D_{air} + x_3u - \eta_{vol}(x_1, N_e)\beta_{int}x_1\right) \\ \dot{x}_2 = \frac{\alpha_{int}}{x_1}\left(F_{exh}x_3u - (D_{air} + x_3u)x_2\right) \\ \dot{x}_3 = 0 \\ y = x_1 \end{cases} \quad (4)$$

Notations are summarized in Table 2.

Var.	Symb.	Var.	Symb.
x_1	P_{int}	y	P_{int}
x_2	F_{int}	α_{int}	$\frac{RT_{int}}{V_{int}}$
x_3	Θ_{egr}	β_{int}	$\frac{1}{RT_{int}}V_{cyl}\frac{N_e}{120}$

TABLE 2

Variables description for the isothermal observer.

4.2 Observer Design

The observer dynamics are

$$\begin{cases} \dot{\hat{x}}_1 = \alpha_{int}\left(D_{air} + \hat{x}_3u - \eta_{vol}(y, N_e)\beta_{int}\hat{x}_1\right) \\ \qquad\qquad -L_1(\hat{x}_1 - y) \\ \dot{\hat{x}}_2 = \frac{\alpha_{int}}{y}\left(F_{exh}\hat{x}_3u - (D_{air} + \hat{x}_3u)\hat{x}_2\right) \\ \dot{\hat{x}}_3 = -L_3(\hat{x}_1 - y) \end{cases} \quad (5)$$

with $(L_1, L_3) \in (\mathbb{R}^+ \setminus \{0\})^2$. One can notice that (5) is a copy of (4) with additive tracking terms. Unknowns are partially substituted with output measurement. The state-error is $\tilde{x} \triangleq x - \hat{x}$. Classically, the error dynamics are

$$\begin{cases} \dot{\tilde{x}}_1 = \alpha_{int}\left(\tilde{x}_3u - \eta_{vol}(y, N_e)\beta_{int}\tilde{x}_1\right) - L_1\tilde{x}_1 \\ \dot{\tilde{x}}_2 = \frac{\alpha_{int}}{y}\left(F_{exh}\tilde{x}_3u - (D_{air} + \hat{x}_3u)\tilde{x}_2 + (F_{exh} - x_2)\tilde{x}_3\right) \\ \dot{\tilde{x}}_3 = -L_3\tilde{x}_1 \end{cases}$$

Tuning parameters are chosen as follows

$$\begin{cases} L_1 = (l_1 - \eta_{vol}(y, N_e))\alpha_{int}\beta_{int} \\ L_3 = l_3\alpha_{int}u \end{cases}$$

where l_1 and l_3 are positive constants. With this choice, the error system writes under the triangular form (6)-(7)

$$\begin{bmatrix} \dot{\tilde{x}}_1 \\ \dot{\tilde{x}}_3 \end{bmatrix} = A_{int}\begin{bmatrix} \tilde{x}_1 \\ \tilde{x}_3 \end{bmatrix} \quad (6)$$

where

$$A_{int} \triangleq \begin{bmatrix} -l_1\alpha_{int}\beta_{int} & \alpha_{int}u \\ -l_3\alpha_{int}u & 0 \end{bmatrix}$$

and

$$\begin{aligned} \dot{\tilde{x}}_2 = {} & \frac{\alpha_{int}}{y}\left(F_{exh}\tilde{x}_3u - (D_{air} + \hat{x}_3u)\tilde{x}_2\right) \\ & + \frac{\alpha_{int}}{y}(F_{exh} - x_2)\tilde{x}_3 \end{aligned} \quad (7)$$

Tuning and convergence of the proposed observer around fixed operating point has been investigated in [14] resulting in the following proposition.

Proposition 1 *For any fixed operating point, i.e. constant values of F_{exh}, T_{int}, N_e, and $u > 0$, the state of observer* (5) *exponentially converges towards the state of system* (4).

5 AIR PATH CONTROL FEEDFORWARD

Now, we have an estimation of the EGR flow and the BGR in the intake manifold. Thanks to that well defined change

of variables, the control inputs are the EGR flow D_{egr} and the fresh air flow D_{air}. The reference model for the control writes

$$\begin{cases} \dot{x}_1 = \alpha_{int}\,(u_1 + u_2 - \eta_{vol}(x_1, N_e)\beta_{int}x_1) \\ \dot{x}_2 = \frac{\alpha_{int}}{x_1}\,(F_{exh}u_2 - (u_1+u_2)x_2) \end{cases} \tag{8}$$

We propose a motion planning control strategy which rely on the computation of transient trajectories for the airpath dynamics (8). This strategy is detailed in Figure 2. It comprises 4 sub procedures: setpoint computations through static maps (first two blocks in Figure 2), trajectory generation, model inversion, and saturation of open-loop control values. We now detail these in the next subsection, we actually prove convergence of the airpath system when using this strategy.

5.1 Set points

The driver's request considered here is the accelerator position. First, taking into account the gear box configuration, this request is turned into a torque control objective under the form of an IMEP (Indicated Mean Effective Pressure) set point. Then, the set points for the intake pressure and the BGR (noted x^{sp} in Figure 2) are inversely given by experimentally calibrated static maps on the $(\mathrm{IMEP}^{\mathrm{sp}}, N_e)$ operating range. The engine speed N_e is not modelled but directly measured. The $x^{\mathrm{sp}} = (x_1^{\mathrm{sp}}, x_2^{\mathrm{sp}})$ vector is defined as

$$x_1^{\mathrm{sp}} = f_{\mathrm{pressure}}(\mathrm{IMEP}^{\mathrm{sp}}, N_e) \quad \text{and} \quad x_2^{\mathrm{sp}} = f_{\mathrm{bgr}}(\mathrm{IMEP}^{\mathrm{sp}}, N_e)$$

5.2 Motion planning

Because $\mathrm{IMEP}^{\mathrm{sp}}$ is arbitrarily specified by the driver, $t \mapsto x_1^{\mathrm{sp}}(t)$ and $t \mapsto x_2^{\mathrm{sp}}(t)$ may not be smooth nor monotonous. These signals must be filtered to correspond to feasible trajectories of (8). This can be done by many methods. Here, we propose the following approach that, besides other interesting properties, is easy to handle in the convergence analysis process. It addresses only the case of transients from one steady state to another. From a current steady state $\underline{x}$ to a target $\overline{x}$ we use an interpolation formula (9). Coordinate-wise this defines x_1^{mp} and x_2^{mp}. Let

$$\phi(t,T) = \begin{cases} 0 & \text{for } 0 \geq t \\ (\frac{t}{T})^2(3 - 2\frac{t}{T}) & \text{for } 0 \leq t \leq T \\ 1 & \text{for } T \leq t \end{cases} \tag{9}$$

Note two positive constants T_1 and T_2. The considered interpolation is

$$\begin{cases} x_1^{\mathrm{mp}}(t) = \underline{x}_1 + (\overline{x}_1 - \underline{x}_1)\phi(t, T_1) \\ x_2^{\mathrm{mp}}(t) = \underline{x}_2 + (\overline{x}_2 - \underline{x}_2)\phi(t, T_2) \end{cases} \tag{10}$$

5.3 Model inversion

System (8) is fully actuated and invertible. Thus, an analytic expression of the input can be derived from the state variables and their first derivatives histories. In fact,

$$\begin{cases} u_1 + u_2 = \eta_{vol}(x_1, N_e)\beta_{int}x_1 + \frac{1}{\alpha_{int}}\dot{x}_1 \\ -x_2u_1 + (F_{exh} - x_2)u_2 = \frac{1}{\alpha_{int}}\dot{x}_2x_1 \end{cases} \tag{11}$$

This rewrites

$$\begin{cases} u_1 = f_1(x, \dot{x}) \\ u_2 = f_2(x, \dot{x}) \end{cases} \tag{12}$$

with

$$\begin{cases} f_1(x,\dot{x}) = \frac{1}{F_{exh}}\Big(\frac{F_{exh}-x_2}{\alpha_{int}}\dot{x}_1 - \frac{1}{\alpha_{int}}\dot{x}_2x_1 \\ \qquad\qquad +(F_{exh} - x_2)\eta_{\mathrm{vol}}(x_1, N_e)\beta_{int}x_1\Big) \\ f_2(x,\dot{x}) = \frac{1}{F_{exh}}\Big(\frac{1}{\alpha_{int}}x_2\dot{x}_1 \\ \qquad\qquad +\eta_{\mathrm{vol}}(x_1, N_e)\beta_{int}x_2x_1 + \frac{1}{\alpha_{int}}\dot{x}_2x_1\Big) \end{cases} \tag{13}$$

In these last expressions, F_{exh}, α_{int}, N_e, and β_{int} are all given by sensors measurements. The unique open-loop control law $(u_1^{\mathrm{mp}}, u_2^{\mathrm{mp}})$ corresponding to any desired $(x_1^{\mathrm{mp}}, x_2^{\mathrm{mp}})$ trajectory (defined by formulas (10)) is

$$\begin{cases} u_1^{\mathrm{mp}} = f_1(x_1^{\mathrm{mp}}, \dot{x}_1^{\mathrm{mp}}, x_2^{\mathrm{mp}}, \dot{x}_2^{\mathrm{mp}}) \\ u_2^{\mathrm{mp}} = f_2(x_1^{\mathrm{mp}}, \dot{x}_1^{\mathrm{mp}}, x_2^{\mathrm{mp}}, \dot{x}_2^{\mathrm{mp}}) \end{cases} \tag{14}$$

5.4 Input constraints

There are several constraints that need to be considered. Input signals (u_1, u_2) and the aspirated flow $(u_1 + u_2)$ must be positive and strictly positive, respectively, because they correspond to input flows. Also, the inputs must not cause misfires (usually due to high EGR). A simple strategy can address this issue. Conservatively, misfire avoidance can be guaranteed provided the following input constraints are satisfied

$$C(u) \triangleq F_{exh}\frac{u_2}{u_2 + u_1} \leq \overline{C} < 1$$

$C(u)$ is equivalent to the BGR at steady state. Adding the previously discussed positiveness of input flows, the set of admissible inputs is defined as

$$\mathcal{U} \triangleq \big\{(u_1,u_2) \in (\mathbb{R})^2 / u_1 + u_2 \geq u_{min},\ \ u_2 \geq 0, \\ \text{and } F_{exh}\frac{u_2}{u_2+u_1} \leq \overline{C}\big\}$$

and we note $\partial\mathcal{U}$ its boundary. We define the constrained control as

$$u^{\mathrm{ol}}(t) \triangleq arg(\min_{u\in\mathcal{U}}\ (u_1 - u_1^{\mathrm{mp}}(t))^2 + (u_2 - u_2^{\mathrm{mp}}(t))^2) \tag{15}$$

where $u_1^{\mathrm{mp}}(t)$ and $u_2^{\mathrm{mp}}(t)$ are defined by (14). A representation of the input constraints in the plane is given in Figure 1. In other words, for all $t \in \mathbb{R}^+$, $u^{\mathrm{ol}}(t)$ is the projection of $u^{\mathrm{mp}}(t) = (u_1^{\mathrm{mp}}, u_2^{\mathrm{mp}})(t)$ onto the set $\mathcal{U}$. In (15),

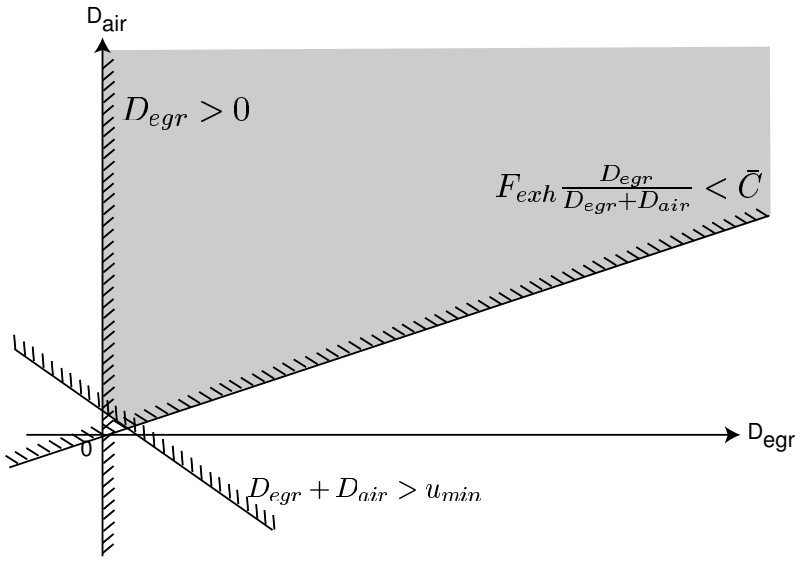

Figure 1

Input constraints in the plan $(u_1 = D_{air}, u_2 = D_{egr})$, the admissible set $\mathcal{U}$ is represented in grey.

both the cost function and the admissible set $\mathcal{U}$ are convex. Thus, there always exists a uniquely defined minimum u^{ol}. In fact, this solution can be analytically, computed in a straightforward way (by enumerating 6 possible solutions), which is compatible with our real-time control application requirements.

5.5 Convergence and tuning of the constrained motion planning

We now prove that the proposed control strategy actually converges. The main focus is on the impact of input saturations as previously described.

It is assumed that the volumetric efficiency slowly varies w.r.t. the intake pressure x_1. Denoting $h(x_1, N_e) \triangleq \eta_{vol}(x_1, N_e)x_1$, we suppose that there exists a strictly positive constant $\bar{h}$ such that for all (x_1, N_e) in $\mathbb{R}^+ \times [500, 4500]$,

$$\frac{\partial h}{\partial x_1}(x_1, N_e) \geq \bar{h} > 0$$

Experimentally, this assumption is actually easy to validate.

5.5.1 Exponential stability

In [15], stability was studied by exploiting the cascade structure of equations (8) leading to the following proposition.

Proposition 2 *Consider system* (8)*. For any constant input* $u = (\bar{u}_1, \bar{u}_2)$*, the state* x *exponentially converges toward* $z \triangleq (z_1, z_2)$ *where* $h(z_1, N_e) = \bar{u}_1 + \bar{u}_2$ *and* $z_2 = F_{exh}\frac{\bar{u}_2}{\bar{u}_1+\bar{u}_2}$*. A way to asymptotically reach* $\bar{x} = (\bar{x}_1, \bar{x}_2)$ *is to use a constant input* $\bar{u}$ *as defined in* (16)*.*

Conversely, it is possible to tune the input values to reach a desired set point $\bar{x} = (\bar{x}_1, \bar{x}_2)$. For that purpose, one should use

$$\begin{cases} \bar{u}_1 = \frac{F_{exh}-\bar{x}_2}{F_{exh}}\eta_{\text{vol}}(\bar{x}_1, N_e)\beta_{int}\bar{x}_1 \\ \bar{u}_2 = \frac{1}{F_{exh}}\eta_{\text{vol}}(\bar{x}_1, N_e)\beta_{int}\bar{x}_1\bar{x}_2 \end{cases} \tag{16}$$

This proposition is the key to understanding our approach. Provided chosen control values are feasible (i.e. belong to $\mathcal{U}$), it is sufficient to use them as the step inputs in the airpath system to asymptotically reach the desired set point. Now, as we mentioned it in the Introduction, our goal is to provide more efficient transients. Ideally, we would like to have soft landings and fast transients. If the proposed control (14) are feasible, then $u^{\text{mp}}(t) = u^{\text{ol}}(t)$ for all $t \in \mathbb{R}^+$ and, neglecting possible perturbations, the transient is perfectly achieved. Yet, if the motion planning strategy is, at times, inconsistent with the input constraints, then $u^{\text{mp}}(t) \neq u^{\text{ol}}(t)$ during the transient. In any cases, for large values of t ($t \geq \max\{T_1, T_2\}$ as used in (9)), both coincide again and equal the feasible final input values. Ultimately, the system converges. The motion planning strategy can only improve transients when the computed input values are feasible, at least over some reasonably long period of the transient interval.

We now perform some analysis that allows us to guarantee this desired feasibility. From this, we can derive guidelines to tune parameters T_1 and T_2.

5.5.2 Transient tuning

In [15], we showed that for large enough values for T_1 and T_2, the control values do not violate the constraints. Moreover, we proved that for small enough values for T_1 and T_2,

the control values do violate the constraints. Constructive choices for T_1 and T_2 in both cases are also given. Consider the motion planning strategy (14) aiming at steering the system from steady state $(\underline{x}, \underline{u}) \in \mathcal{U}$ to $(\overline{x}, \overline{u}) \in \mathcal{U}$. From this performance analysis, we can propose the following tuning methodology for T_1 and T_2

1. We choose $\epsilon_1 > 0$ and pick $T_1 = \frac{2}{\epsilon_1}\frac{|\overline{x}_1 - \underline{x}_1|}{\alpha_{int}}$ to account for turbocharger inertia (which drives the air flow dynamics).
2. We choose $\epsilon_2 > 0$ and use

$$T_2 = \max\{T_2 \in [T_m(T_1), T_M(T_1, \epsilon_2)]/ \\ \forall t \in \mathbb{R}^+ dist(u^{\mathrm{mp}}(t), \mathcal{U}) < \epsilon_2\}$$

where

$$\begin{cases} T_m(T_1) & \triangleq \dfrac{|\overline{x}_2 - \underline{x}_2|}{\Phi_{int}\overline{\eta_{vol}} + \frac{3|\overline{x}_1 - \underline{x}_1|}{2T_1 \max\{\overline{x}_1, \underline{x}_1\}}} \\ T_M(T_1, \epsilon_2) & \triangleq \dfrac{2}{\epsilon}\dfrac{|\overline{x}_2 - \underline{x}_2|}{\Phi_{int}\underline{\eta_{vol}} - \frac{3|\overline{x}_1 - \underline{x}_1|}{2T_1 \min\{\overline{x}_1, \underline{x}_1\}}} \end{cases}$$

These rules guarantee that the constraints are not violated by more than $\max\{\epsilon_1, \epsilon_2\}$.

6 AIR PATH CONTROL FEEDBACK

Fast PID controllers are added to the structure to provide further accuracy and robustness. The goal of the feedback is to control the EGR flow D_{egr} and the air flow D_{air} toward the reference setpoints D_{egr}^{ol} and D_{air}^{ol}. The main purpose of the feedforward is to give a feasible and continuous setpoint for the feedback action.

6.1 EGR position to D_{egr}

Increasing the EGR position corresponds to opening the EGR valve and, thereby, increasing the EGR flow D_{egr}. The flow response is almost instantaneous, the EGR valve opening control the EGR flow D_{egr}. More precisely, a PI controller with an anti-wind up action on the normalized EGR flow ($\frac{D_{\mathrm{egr,sp}} - \hat{D}_{\mathrm{egr}}}{\hat{\Theta}_{egr}}$) is used on the EGR valve.

6.2 EGR/VGT to D_{air}

Increasing the VGT position, i. e. opening the guide vanes, leads to a greater restriction of the exhaust gas flow and then to a decrease of the exhaust manifold pressure.

When the EGR valve is wide open (at low speed and low load e.g.), increasing the VGT results in a decreased EGR flow D_{egr} which in turn increases the air flow D_{air}.

When the EGR valve is almost closed, most of the exhaust gas must pass through the turbine. Increasing the VGT decreases the compressor power and, then, increases the air flow. In this case, the VGT acts as a conventional wastegate, i.e. the VGT directly controls the turbocharger speed and the air flow D_{air}. Therefore, the steady-state gain from VGT to D_{air} undergoes a sign change depending on the operating point. Since it is uncertain where the sign change occurs, the VGT should not be used to track D_{air} setpoints in a decentralized strategy. Rather, the strategy should use the EGR flow information. The variation of intake pressure is monotonic w.r.t. VGT. Depending on the opening of the EGR valve, i.e. depending on the EGR flow, the variation of pressure is very different. Indeed, in practice, with very high EGR rate, the variation of the VGT slightly impact the intake pressure. A tedious calibration work is a solution.

Low EGR		
Decreasing VGT	⇒	High increasing D_{air}
	⇒	Low increasing D_{egr}
High EGR		
Decreasing VGT	⇒	Low decreasing D_{air}
	⇒	Low increasing D_{egr}

TABLE 3

Variation of air/egr flows depending on VGT

7 EXPERIMENTAL RESULTS

7.1 Implementation

The global control scheme is summarized in Figure 2. The air path observer block (Block (A)) is the implementation of the observer described in Section 4. This block gives an estimation of the BGR and the EGR flow. The motion planning block (Block (B)) is the implementation of the motion planning open loop control strategy described in Section 5. Fast PID controllers are added to the structure (Block (C)) to provide further accuracy and robustness. Their implementation is described in Section 6.

The control was tested on torque trajectory at fixed engine speed (1500 rpm). This torque trajectory mixes HCCI combustion mode (for $\mathrm{IMEP}_{sp} < 7$ bar) and conventional combustion mode. The same calibration was kept on all the torque trajectory. The IMEP demand is given in Figure 3. On IMEP transient in HCCI mode, it occurs that we want to increase both BGR and intake pressure. This is the case when IMEP of the system starts at 2 bar and eventually reaches 5 bar (from $t = 102$s to $t = 112$s). This transient aims higher intake pressure and BGR setpoints. Starting and ending operating points are both in HCCI combustion mode. Let us focus on Figures 6 and 7 (from $t = 102$s to $t = 112$s). By contrast with all decentralized controllers, we notice on that our controller takes into account the well known non minimum phase behavior of the system reported in [3]. More precisely, one can check that the main contribution to this is due to the open-loop controller (the closed

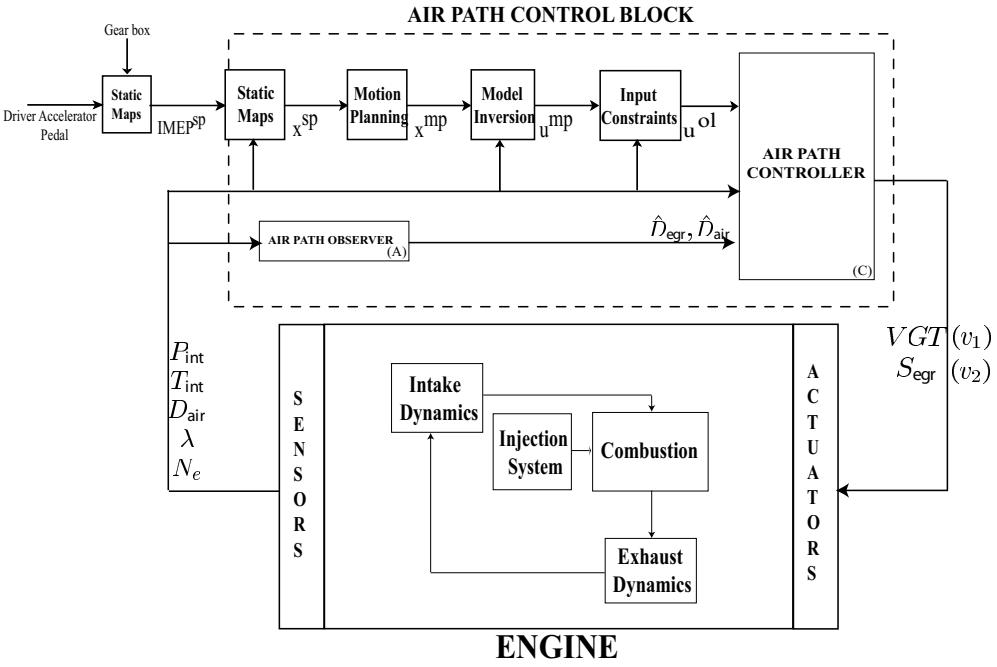

Figure 2

Control Scheme

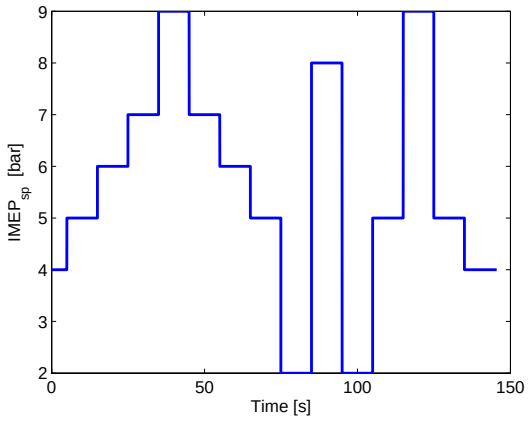

Figure 3

Torque trajectory at constant engine speed (1500 rpm).

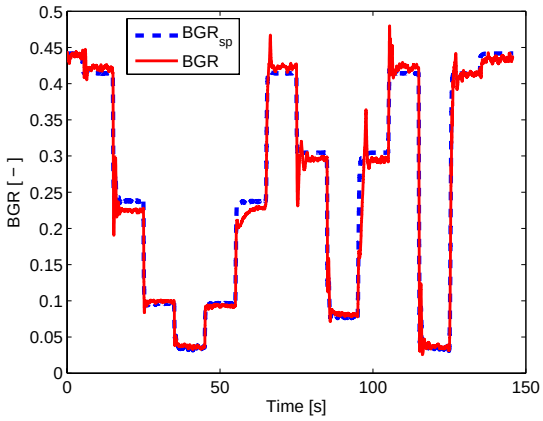

Figure 4

Experimental results on a torque trajectory at constant engine speed (1500 rpm): BGR histories. Dashed : set point, solid: closed-loop trajectory.

loop control histories being very close to it). When the EGR valve opens, the flow increases. This leads to a pressure rise in the intake manifold. Meanwhile, the exhaust pipe acts as a discharge for the VGT. Its opening lowers the EGR supplied to the turbocharger yielding a significant drop of the exhaust manifold flow. The turbocharger slows down, which eventually causes the decrease of the intake manifold pressure. This phenomenon is delayed and slowed down by the turbocharger inertia. Simple ramps and/or steps would fail to let the system reach the desired setpoint. With the proposed control strategy, the model takes into account this complex behavior. The motion planning efficiently drives the system to its setpoint.

The air and EGR flows setpoints and closed-loop trajectory are presented on Figures 6 and 7. As in the following cases, the EGR flow is almost perfectly tracked, the air flow tracking is good but a little bit slow during large transients

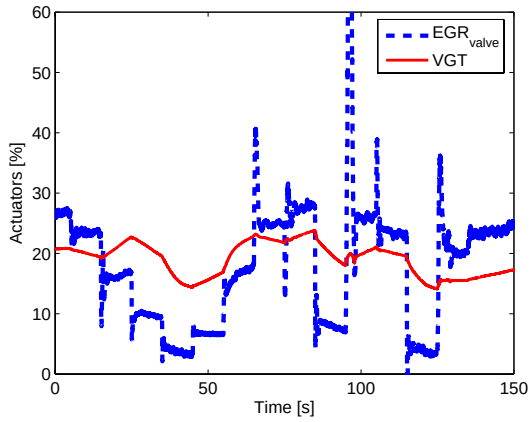

Figure 5

Experimental results on a torque trajectory at constant engine speed (1500 rpm): Actuators histories. Dashed : EGR valve, solid: VGT.

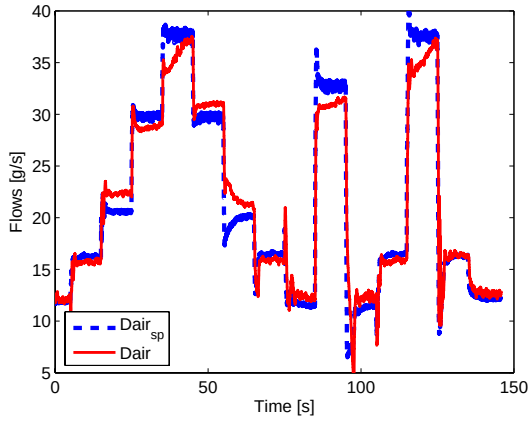

Figure 6

Experimental results on a torque trajectory at constant engine speed (1500 rpm): Air flow histories. histories. Dashed : set point, solid: closed-loop trajectory.

due to the turbocharger inertia. In summary, the results are good, even with a reasonably large transient. We are able to follow the planned trajectory. High pressure setpoints are more difficult to reach due to the turbocharger inertia and friction. However, it is possible to relax the intake pressure tracking because, for pollutant reduction purposes, only BGR needs to be closely controlled provided a limited Air-Fuel Ratio is guaranteed. The errors on the intake pressure will only lead to a very small error on the torque production. Nevertheless, on a vehicle, this problem will not appear because as the torque production increases, in response, the engine speed and the turbocharger speed increases. This phenomenon is expected to be reduced in real-vehicle applications.

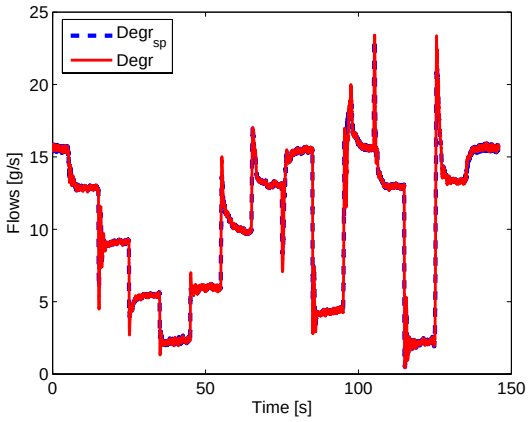

Figure 7

Experimental results on a torque trajectory at constant engine speed (1500 rpm): EGR flow histories. histories. Dashed : set point, solid: closed-loop trajectory.

8 CONCLUSIONS AND FUTURE WORK

8.1 Conclusion

The presented work demonstrates the relevance of motion planning in the control of the –coupled– airpath dynamics of turbocharged Diesel engines using Exhaust Gas Recirculation. For the HCCI combustion mode, very large rates of burned gas need to be considered and we have proven on realistic test-bench cases that the proposed approach can handle such situations. Despite strong coupling and possible nonminimum phase dynamics, the airpath dynamics has nice properties that make it easy to steer through our control strategy. Its triangular form yields exponential convergence over a wide range of setpoints. Moreover, we showed that input constraints can be added without jeopardizing convergence.

8.2 Toward general airpath control

The presented work is validated experimentally on a HCCI engine with a high pressure EGR circuit and a Variable Geometry Turbocharger. The next step is the extension of the control strategy to other engine configurations, e.g. considering low pressure EGR circuit, waste-gate, two-stage turbocharger, intake throttle ... The control strategy can be kept. The observer will be the same (Block (A) in Figure 2), and so will the motion planning. The main modification will be to decentralize the control in order to use all the actuators for the control of the air flow D_{air} and the EGR flow D_{egr}.

REFERENCES

[1] J. Kahrstedt, K. Behnk, A. Sommer, and T. Wormbs. Combustion processes to meet future emission standards. In *Motortechnische Zeitschrift*, pages 1417–1423, 2003.

[2] A. Hultqvist, U. Engdar, B. Johansson, and J. Klingmann. Reacting boundary layers in a homogeneous charge compression ignition (HCCI) engine. In *Proc. of the SAE Conference*, number 2001-01-1032, 2001.

[3] I. Kolmanovsky, A. Stefanopoulou, P. Moraal, and M. van Nieuwstadt. Issues in modelling and control of intake flow in variable geometry turbocharged engines. In *Proc of the 18^{th} IFIP Conference on System Modelling and Optimization*, 1997.

[4] M. Kao and J. Moskwa. Turbocharged Diesel engine modelling for nonlinear engine control and estimation. *ASME Journal of Dynamic Systems, Measurements and Control*, 117, 1995.

[5] M. van Nieuwstadt, P. Moraal, I. Kolmanovsky, A. Stefanopoulou, P. Wood, and M. Criddle. Decentralized and multivariable designs for EGR-VGT control of Diesel engine. In *Proc of the 2^{nd} IFAC Workshop on Advances in Automotive Control*, 1998.

[6] A. Stefanopoulou, I. Kolmanovsky, and J. Freudenberg. Control of variable geometry turbocharged Diesel engines for reducted emissions. *IEEE Transactions on Control Systems Technology*, 8:733–745, 2000.

[7] M. van Nieuwstadt, I. Kolmanovsky, P. Moraal, A. Stefanopoulou, and M. Janković. Experimental comparison of EGR-VGT control schemes for a high speed Diesel engine. *Control System Magazine*, 20:63–79, 2000.

[8] M. Jung and K Glover. Control-oriented linear parameter-varying modelling of a turbocharged Diesel engine. 2003.

[9] M. Jung and K Glover. Comparison of uncertainty parameterisations for H-infinity robust control of turbocharged Diesel engines. 13:15–25, 2005.

[10] M. Ammann, N. Fekete, L. Guzzella, and A. Glattfelder. Model-based control of the VGT and EGR in a turbocharged common-rail Diesel engine: theory and passenger car implementation. In *Proc. of the SAE Conference*, number 2003-01-0357, 2003.

[11] M Janković and I. Kolmanovsky. Robust nonlinear controller for turbocharged Diesel engine. In *Proc. of the American Control Conference*, 1998.

[12] M Janković and I. Kolmanovsky. Constructive Lyapounov control design for turbocharged Diesel engines. *IEEE Transactions on Control Systems Technology*, 8:288–299, 2000.

[13] J. Heywood. *Internal Combustion Engine Fundamentals*. McGraw-Hill, Inc, 1988.

[14] J. Chauvin, G. Corde, C. Vigild, N. Petit, and P. Rouchon. Air path estimation on Diesel HCCI engine. In *Proc. of the SAE Conference*, number 2006-01-1085, 2006.

[15] J. Chauvin, G. Corde, and N. Petit. Constrained motion planning for the airpath of a Diesel HCCI engine. In *Proc. of the IEEE Conf. Decision and Control*, 2006.